Pressure Swing Adsorption for Biogas Upgrading. Effect of Recycling Streams in Pressure Swing Adsorption Design

Mónica P. S. Santos, Carlos A. Grande,* and Alírio E. Rodrigues

Laboratory of Separation and Reaction Engineering (LSRE), Associate Laboratory LSRE/LCM, Department of Chemical Engineering, Faculty of Engineering, University of Porto, Rua Dr. Roberto Frias, s/n, 4200-465, Porto, Portugal

The upgrading of biogas by pressure swing adsorption (PSA) was studied. Simulations of a process for binary separation of CH_4-CO_2 using zeolite 13X as selective adsorbent were carried out at 323 K. The results obtained with a two-column PSA process using a six-step cycle (pressurization, feed, depressurization, blowdown, purge, and pressure equalization) were compared with initial estimates by simulating the behavior of only one column. The recycle of highly contaminated streams was quantitatively evaluated in this paper. When recycled streams have purity lower than 99%, there is a significant decrease in the overall purity of biomethane. According to the simulations performed for a stream of biogas of 500 N m^3/day, it is possible to obtain biomethane with a purity higher than 99% with a recovery of 85% and a power consumption of 0.12 kW/mol of produced methane.

1. Introduction

Methane (CH_4), like carbon dioxide (CO_2) gas, is a significant contributor to the accumulation of greenhouse gases (GHG) and consequently for increased global warming:[1] the greenhouse warming potential (GWP) of methane is 21 times higher than that for CO_2.[2] Principal sources of methane emissions to atmosphere are natural gas systems, enteric fermentation, landfills, and wastewater treatment plants. Tighter control in methane emissions will have a significant contribution in mitigating anthropogenic emissions.

Landfill gas (LFG) and the biogas generated in anaerobic digestion units of wastewater treatment plants (WWTPs) are the main sources of methane emissions in several countries.[3] Considering that this methane can also be used for energy or fuel production, this is a win-win situation for the generation of a biofuel. For this reason, it is the biofuel with higher tons of CO_2 avoided.[4]

The use of biomethane as fuel or its injection in a pipeline for grid distribution introduces some quality specifications for biogas. Despite the removal of several contaminants (siloxanes, H_2S), the gas should have a very small content of water and carbon dioxide concentration below 2−3%.[5] From all these separations, CH_4-CO_2 is the most expensive one, since normally CO_2 content is higher than 25%. The biogas composition of LFG depends on the waste composition and aging of the landfill.[6] The composition of biogas generated in anaerobic digestion units of WWTPs depends on the sludge and the operation conditions of the digestion process. Humidity, pH, temperature, composition, and particle size and age of the waste are factors that affect the biogas generation.

After the removal of minor contaminants, carbon dioxide and methane can be separated by physical or chemical scrubbing,[7,8] membrane-based processes,[9] pressure swing adsorption (PSA), and temperature swing adsorption (TSA).[2,10−13]

PSA technology can operate in two distinct modes, depending on the adsorbent employed.[12,14,15] Some materials present stronger surface interactions with CO_2, adsorbing larger loadings of this gas when compared to methane. These materials are termed as equilibrium-based adsorbents, and some examples are activated carbon,[16−18] zeolite 13X,[19] silica gel,[20] and metal−organic frameworks.[21,22] Other materials (like carbon molecular sieves,[23] clinoptilolites,[24−26] titanosilicates,[27,28] DDR zeolites,[29] and SAPO-34[30]) have similar adsorption loadings of CO_2 and CH_4. In these adsorbents, the diffusion rate is controlled by tightening the size of the micropores and more CO_2 is retained per unit time, resulting in a kinetic separation.

There are several studies of CH_4/CO_2 separation, where the separation was performed with adsorbents that allow operating under the kinetic-control regime.[12,15,31−38] There are also few studies, for the same mixture, operating with equilibrium adsorbents.[12,13,39,40] Four (Skarstrom cycle[41]) or five steps single bed were considered in these studies mentioned. We have previously demonstrated that kinetic-based adsorbents may result in higher overall productivities than equilibrium-based adsorbents.[12] The main reason for that was the strong nonlinearity of the isotherms of equilibrium-based adsorbents such as zeolites.[15] However, the performance of equilibrium-based materials can be improved if higher temperatures are employed.

The objective of this work is to demonstrate that equilibrium-based adsorbents can significantly contribute to biomethane production from thermophilic digestors where the temperature is around 323 K.[42] The feed conditions were fixed: 500 m^3/day (measured in standard conditions, 296.15 K and 1 atm), available at 323 K and with 67% of CH_4 and 33% CO_2. Several PSA simulations were performed to obtain a product (CH_4) with over 98% purity and high recovery. The influence of multicolumn operation was studied using a modified Skarstrom cycle comprising co-current pressurization with feed, feed, co-current pressure equalization depressurization, counter-current blowdown, counter-current purge with product, and counter-current pressure equalization pressurization. The introduction of an equalization step introduced a great improvement in the PSA process.[43−47] The design of a PSA unit can be done by studying the performance of one column and avoiding recycling of gases from other columns. The effect of recycling dirty streams was evaluated, since the objective is to produce methane with 98% purity (contamination of CO_2 may achieve 2%).

* To whom correspondence should be addressed. Telephone: +351 22 508 1618. Fax: +351 22 508 1674. E-mail: cgrande@fe.up.pt.

10.1021/ie100757u
Published on Web 12/15/2010

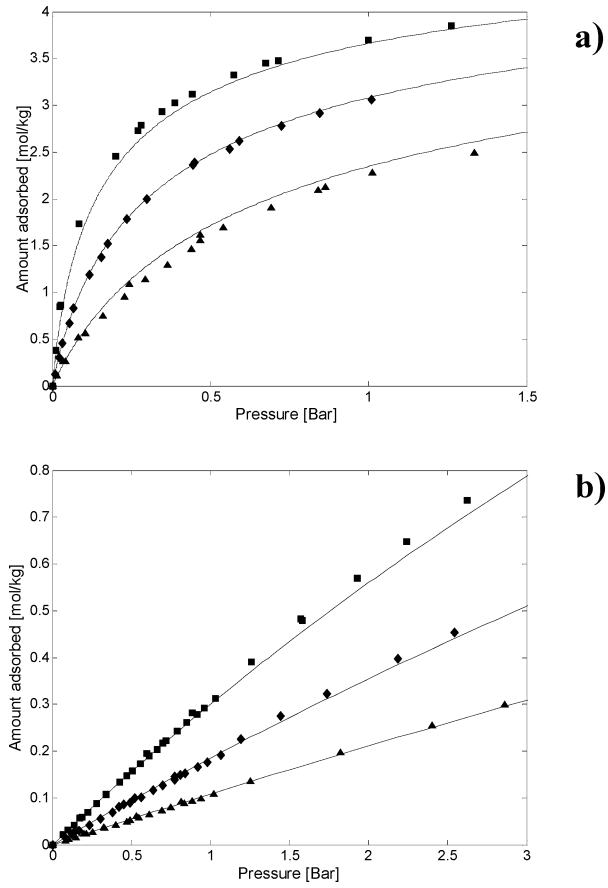

Figure 1. Adsorption equilibrium isotherms on zeolite 13X of (a) CO_2 and (b) CH_4: (■) $T = 303$, (◆) $T = 323$, and (▲) $T = 348$ K.

2. Pressure Swing Adsorption Simulations

A classical PSA unit is composed of several columns operating in parallel filled with one selective adsorbent. However, the configuration of PSA units is so flexible that we can find units with only one column[48] or with multiple adsorbents per column.[13,49−52]

When a PSA unit is designed for an application, the first difficulty to overcome is the selection of the adsorbent. As mentioned before, kinetic adsorbents are normally selected for bulk separation of CO_2. Nonetheless, it was mentioned by several researchers that zeolite adsorbents can also provide an alternative. In this work, zeolite 13X was selected since operating at 323 K the isotherm steepness is reduced and faster regeneration can be carried out.

2.1. Adsorption Equilibrium and Kinetics. The first part of this work was related to basic characterization of a zeolites sample. We have determined adsorption equilibrium in a magnetic suspension balance (Rubotherm, Germany). The adsorption equilibrium of CO_2 and CH_4 is reported in Figure 1.

Solid lines in Figure 1 correspond to the fitting of the multisite Langmuir model.[53] The multisite Langmuir model represented in eq 1 assumes that a molecule can occupy more than one adsorption site of a homogeneous surface. This model is given by

$$\left(\frac{q_i^*}{q_{i,\max}}\right) = a_i K_i P y_i \left[1 - \frac{q_i^*}{q_{i,\max}}\right]^{a_i} \tag{1}$$

where q_i^* and $q_{i,\max}$ are the current and the maximum amount adsorbed, respectively, of component i for a given pressure P and a constant solid temperature T_s. The exponent a_i corresponds to the number of neighboring sites that a molecule can occupy. The adsorption constant (K_i) is assumed to have an exponential dependence of temperature according to

$$K_i = K_i^0 \exp\left(-\frac{\Delta H_i}{R_g T}\right) \tag{2}$$

where K_i^0 is the infinite adsorption constant and ΔH_i is the heat of adsorption. If we neglect adsorbate−adsorbate interactions, the multicomponent extension of this model can be expressed as

$$\left(\frac{q_i^*}{q_{i,\max}}\right) = a_i K_i P y_i \left[1 - \sum_i \left(\frac{q_i^*}{q_{i,\max}}\right)\right]^{a_i} \tag{3}$$

The saturation capacity of each component is imposed by the thermodynamic constraint, $a_i q_{i,\max} =$ constant to satisfy a material balance of sites in the adsorbent.[54] The parameters obtained from fitting of pure adsorption equilibrium are shown in Table 1.

Normally, diffusion within zeolites crystals can be simplified to a linear driving force (LDF) model. For the case of crystal diffusion, the micropore LDF constant ($k_{u,i}$) assumes the same exponential dependence of temperature[55] as micropore diffusion:

$$K_{u,i} = K_{u,i}^0 \exp\left(-\frac{Ea_i}{R_g T}\right) \tag{4}$$

where $K_{u,i}^0$ is the LDF constant for infinite temperature and E_{ai} is the energy of activation. The micropore LDF constants for micropore diffusion of gases within the zeolite crystals are reported in Table 1.

2.2. Mathematical Modeling of Fixed-Bed Columns. The mathematical model of a column filled with adsorbent is described by a set of partial differential equations including mass, energy, and momentum balances. For some specific cases, these equations can be simplified (constant velocity or isothermal behavior); however, for bulk gas-phase separations, all these equations are normally required.[14,15] In this work, the mathematical model used to describe the fixed-bed adsorption column is based on the following assumptions:[56]

- The gas phase behaves as an ideal gas.
- Mass, heat, and momentum variations in the radial direction are negligible.
- The mass transfer rate is represented by a bilinear driving force (bi-LDF) model.
- A film mass transfer in the layer surrounding the extrudates is considered.
- The pressure drop in the column is described by the Ergun equation.
- The bed porosity is considered constant along the bed.

The component mass balance for the gas phase in the adsorption column is given by

$$\frac{\partial}{\partial z}\left(\varepsilon_c D_{ax} C_T \frac{\partial y_i}{\partial z}\right) - \frac{\partial}{\partial z}(u_0 C_i) = \varepsilon_c \frac{\partial C_i}{\partial t} + \frac{(1-\varepsilon_c) a_p k_{f,i}}{(1 + Bi_i/5)} \times (C_i - \langle C_{p,i} \rangle) \tag{5}$$

where C_T is the total gas-phase concentration, C_i is the gas-phase concentration of component i, D_{ax} is the axial dispersion coefficient, u_0 is the superficial velocity, ε_c is the column porosity, $k_{f,i}$ is the film mass-transfer resistance for component

Table 1. Multisite Langmuir Adsorption Equilibrium Parameters (And Micropore LDF Constant) of CH_4 and CO_2on Zeolite 13X

gas	$q_{i,max}$ (mol/kg)	K_i^0 (kPa^{-1})	$-\Delta H$ (J/mol)	a_i (dimensionless)	E_{ai} (J/mol)	$K_{u,i}^0$ (m^2/s)
CO_2	5.305	2.93×10^{-8}	31 164	1.962	21 008	1.74×10^{-11}
CH_4	6.411	1.29×10^{-8}	20 856	1.624	6621	2.52×10^{-12}

i, $\langle C_{p,i}\rangle$ is the averaged concentration of component i in the macropores of the adsorbent, and a_p is the extrudate specific area.

In this equation, the Biot number of component i is defined as

$$Bi_i = \frac{k_{f,i}R_p^{\,2}}{\varepsilon_p D_{p,i}} \tag{6}$$

where $D_{p,i}$ is the pore diffusivity of component i.

When the LDF approximation is used to describe mass transfer rate within the large pores of the matrix, the mass balance for extrudate is given by

$$\frac{\partial\langle C_{p,i}\rangle}{\partial t} = \frac{15D_{p,i}}{R_p^{\,2}}\frac{1}{(1+5/Bi_i)}(C_i - \langle C_{p,i}\rangle) - \frac{\partial\langle \bar{q}_i\rangle}{\partial t}\frac{\rho_p}{\varepsilon_p} \tag{7}$$

where R_p is the extrudate radius, ρ_p is the particle density, ε_p is the pellet porosity, and $\langle \bar{q}_i\rangle$ is the extrudate-averaged adsorbed-phase concentration of component i. The pore diffusion coefficient, $D_{p,i}$, was estimated assuming contribution of molecular and Knudsen diffusion with a torsuosity factor of 2.0.[56]

The mass transfer rate in micropores is also described by a LDF approximation given by

$$\frac{\partial\langle \bar{q}_i\rangle}{\partial t} = \frac{15D_{c,i}}{r_c^{\,2}}(q_i^* - \langle \bar{q}_i\rangle) = K_{u,i}(q_i^* - \langle \bar{q}_i\rangle) \tag{8}$$

where $D_{c,i}$ is the crystal diffusivity of component i, r_c is the crystal radius, and q_i^* is the gas-phase concentration of component i in equilibrium with the gas concentration within the micropores, $\langle C_{p,i}\rangle$.

The superficial velocity is related to the total pressure gradient by the Ergun equation:

$$-\frac{\partial P}{\partial z} = \frac{150\mu(1-\varepsilon_c)^2}{d_p^{\,2}\varepsilon_c^{\,3}}u_0 + \frac{1.75(1-\varepsilon_c)\rho_g}{d_p\varepsilon_c^{\,3}}|u_0|u_0 \tag{9}$$

where P is the total pressure, μ is the gas viscosity, d_p is the particle diameter, and ρ_g is the gas density.

To take into account the energy transfer, three different balances were employed: gas, solid, and column wall. The energy balance for the gas phase is expressed by

$$\varepsilon_c C_T \tilde{C}_v \frac{\partial T_g}{\partial t} = \frac{\partial}{\partial z}\left(\lambda\frac{\partial T_g}{\partial z}\right) - u_0 C_T \tilde{C}_p \frac{\partial T_g}{\partial z} + \varepsilon_c R_g T_g \frac{\partial C_T}{\partial t} - (1-\varepsilon_c)h_f a_p(T_g - T_s) - \frac{2h_w}{R_w}(T_g - T_w) \tag{10}$$

where $\tilde{C}_v$ is the molar constant volumetric specific heat of the gas mixture, T_g is the temperature of the gas phase, T_s is the solid (extrudate) temperature, T_w is the wall temperature, λ is the axial heat dispersion, $\tilde{C}_p$ is the molar constant pressure specific heat of the gas mixture, h_f is the film heat-transfer coefficient between the gas and solid phases, h_w is the film heat-transfer coefficient between the gas phase and the column wall, and R_w is the column radius.

The energy balance in the solid phase is given by

$$(1-\varepsilon_c)[\varepsilon_p\sum_{i=1}^{n}\langle C_{p,i}\rangle\tilde{C}_{vi} + \rho_p\sum_{i=1}^{n}\langle \bar{q}_i\rangle\tilde{C}_{v,ads,i} + \rho_p\tilde{C}_{ps}]\frac{\partial T_s}{\partial t} = (1-\varepsilon_c)\varepsilon_p R_g T_s\frac{\partial\langle C_{p,i}\rangle}{\partial t} + \rho_b\sum_{i=1}^{n}(-\Delta H_{ads,i})\frac{\partial\langle \bar{q}_i\rangle}{\partial t} + (1-\varepsilon_c)h_f a_p(T_g - T_s) \tag{11}$$

where $\tilde{C}_{p,i}$ is the constant volumetric specific heat of component i, $\tilde{C}_{v,I}$ is the molar constant volumetric specific heat of component i, $\tilde{C}_{v,ads,i}$ is the molar constant volumetric specific heat of component i adsorbed, ρ_b is the bulk density, and $(-\Delta H_i)$ is the isosteric heat of adsorption.

For the column wall, the energy balance is described by

$$\rho_w\tilde{C}_{pw}\frac{\partial T_w}{\partial t} = \alpha_w h_w(T_g - T_w) - \alpha_{wl}U(T_w - T_\infty) \tag{12}$$

where $\tilde{C}_{pw}$ is the specific heat of the column wall, U is the global external heat-transfer coefficient, and T_∞ is the environment temperature. In this equation, α_w is the ratio of the internal surface area to the volume of the column wall and α_{wl} is the ratio of the logarithmic mean surface area of the column shell to the volume of the column wall, that are defined by

$$\alpha_w = \frac{d_{wi}}{e(d_{wi}+e)} \tag{13}$$

$$\alpha_{wl} = \frac{1}{(d_{wi}+e)\ln\left(\frac{d_{wi}+e}{d_{wi}}\right)} \tag{14}$$

The mathematical model proposed was validated against binary breakthrough curves and one-column PSA experimental data using zeolite 13X.[31] The mass and heat parameters employed in this model were estimated using correlations existing in literature.[55,57−59] These correlations are summarized in Table 2.

2.3. Definition of PSA Cycle and Performance Variables. The operation of a PSA unit is cyclic: prior to massive breakthrough of the most adsorbed compound (CO_2), the adsorbent should be regenerated. To handle this requirement in continuous feed processing, several columns are employed: when one column is in feed mode, the other(s) are in regeneration. The regeneration procedure is also performed in different steps, intending to speed up the removal of the adsorbed components.

In this work, the PSA cycle employed was a modified Skarstrom cycle[36] including pressure equalization. The steps are as follows:

1. Co-current pressurization with feed to condition the pressure to start a new cycle.
2. Co-current feed, where selective removal of CO_2 takes place.
3. Co-current pressure equalization depressurization. In this step, the column is partially depressurized and the exiting gas is recycled to other column to save energy.
4. Counter-current blowdown where the pressure is reduced to the lower pressure of the cycle. Removal of CO_2 starts in this step.

Table 2. Correlations Used for Estimation of Mass and Heat Transfer Parameters

axial mass dispersion[55]	$\frac{\varepsilon_c D_{ax}}{D_m} = (20 + 0.5ScRe); \quad Re = \frac{\rho_g u d_p}{\mu_g}; \quad Sc = \frac{\mu_g}{\rho_g D_m}$
axial heat dispersion[57]	$\frac{\lambda}{k_g} = (7.0 + 0.5ScRe); \quad Pr = \frac{\hat{C}p_g \mu_g}{k_g}$
molecular diffusion[55]	$D_{m,i} = (1 - y_i) / \sum_{\substack{j=1 \\ J \neq i}}^{n} \left(\frac{y_i}{D_{Ij}}\right)$
Knudsen diffusion[58]	$D_{k,i} = 9700 r_p \sqrt{\frac{T_g}{M_w}}$
film mass transfer[57]	$Sh = (2.0 + 1.1Re^{0.6}Sc^{1/3}); \quad Sh = \frac{k_g d_p}{D_m}$
film heat transfer[59]	$Nu = (2.0 + 1.1Re^{0.6}Pr^{1/3}); \quad Pr = \frac{h_f d_p}{k_g}$

5. Counter-current purge with product to displace CO_2 from the product-end of the column.
6. Counter-current pressure equalization recycling the gas exiting step 3 from other column to partially increase the pressure of the column.

A schematic representation of this cycle for a single column as well as the pressure history over one cycle is shown in Figure 2. Simplified simulations of PSA cycles are carried out using this one-column scheme: the inlet streams of steps 5 and 6 (purge and pressure equalization) are not recycled from the feed stream avoiding links between different columns and also saving variables making simulations faster. Note that, in the one-column simulations, the gas exiting step 3 is not considered as product and is also not recycled into the column. Also, the inlet streams used in purge and pressure equalization steps were pure methane. The results obtained using this strategy do not have any gas recycled into the column and also let us evaluate the increase of product recovery by using one equalization step.

A more realistic description of the system involves the simulation of all the columns comprised in the PSA unit. For a two-column PSA unit, the schematic representation is given in Figure 3 together with a pressure history. Simulations of multiple columns were performed for H_2 production indicating some variations in the performance.[52,60,61] In this particular case, the specification of 98% purity for CH_4 indicates that the recycled feed stream may contain large amounts of CO_2 which may seriously deviate the behavior of the one-column simulations from real performance.

Four different parameters were used to evaluate the process performance. These parameters are: product (CH_4) purity and recovery, unit productivity and power consumption. Product purity is defined for the stream exiting the feed step by:

$$\text{purity} = \frac{N_{CH_4}}{N_{CH_4} + N_{CO_2}} \tag{15}$$

where N_{CH_4} and N_{CO_2} are the number of moles of methane and carbon dioxide, respectively, that exit the column in the feed step.

The CH_4 recovery is defined by the ratio between the number of moles of methane obtained as product divided by the number of moles of CH_4 introduced in the feed (and pressurization steps).

$$\text{recovery} = \frac{N_{CH_4} - R_{CH_4}}{F_{CH_4}} \tag{16}$$

where R_{CH_4} is the number of moles of methane that is recycled in the purge and pressure equalization steps and F_{CH_4} is the number of moles of methane fed to the column in the feed step.

The CH_4 productivity is calculated by

$$\text{productivity} = \frac{F_{CH_4}\,\text{recovery}}{t_{total} w_{ads}} \tag{17}$$

where t_{total} is the total cycle time and w_{ads} the adsorbent mass.

The power consumption is defined as the required energy for compression of the different streams and the energy requirements of the PSA unit; it is calculated by adiabatic compression given by

$$\text{power consumption} = \left(\frac{\gamma}{\gamma - 1}\right) R_g T_{feed} \left[\left(\frac{P_{high}}{P_{low}}\right)^{\left(\frac{\gamma-1}{\gamma}\right)} - 1\right] \frac{\dot{B}}{1000\eta} \tag{18}$$

where $\gamma = (\tilde{C}_p)/(\tilde{C}_v)$ (equal to 3/2 for ideal gases), R_g is the universal gas constant, P_{high} is the discharge pressure, P_{low} is the suction or blowdown pressure, $\dot{B}$ is the molar flow rate to be compressed, and η is the mechanical efficiency, which typically assumes a value of 0.8. For the compression of methane from 4 to 200 bar, $\gamma = 1.31$ was employed. The power

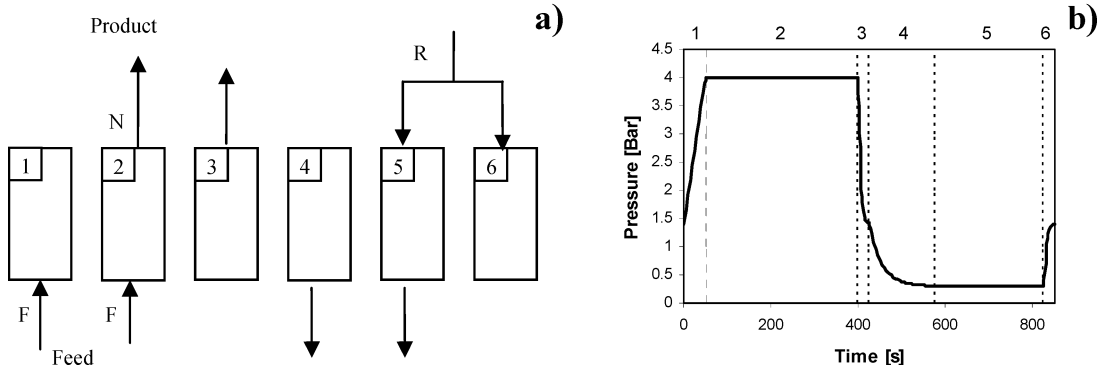

Figure 2. PSA cycle scheme (a) and pressure history of one CSS cycle (b) for a six-step one-column PSA simulation. Steps are (1) co-current feed pressurization, (2) adsorption, (3) co-current pressure equalization depressurization, (4) counter-current blowdown, (5) counter-current purge, and (6) counter-current pressure equalization pressurization.

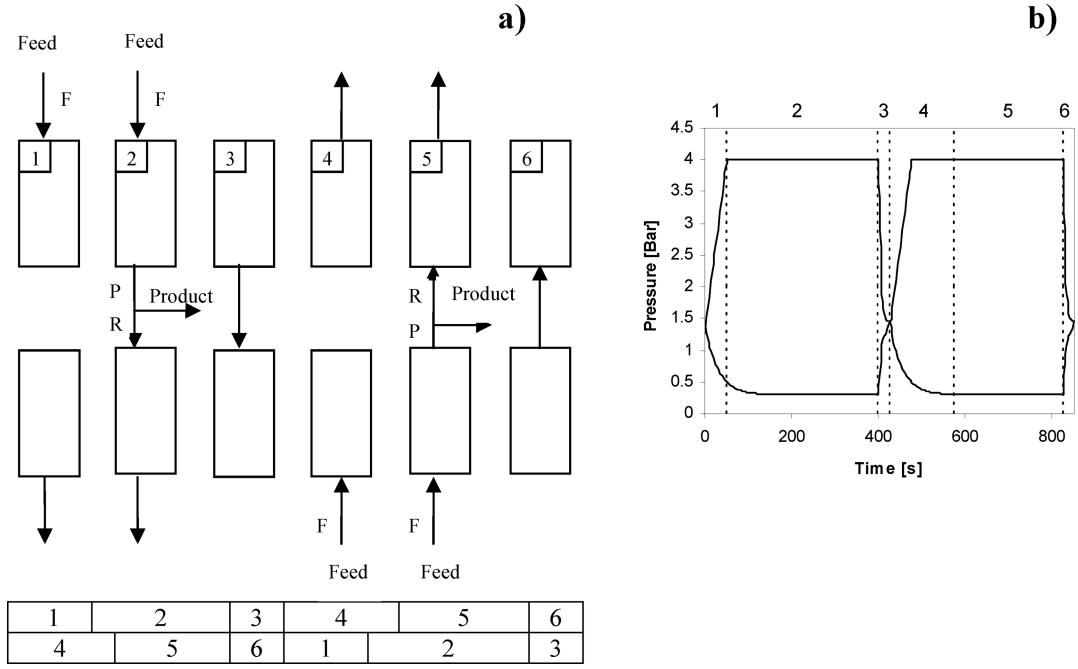

Figure 3. PSA cycle scheme (a) and pressure history of one CSS cycle (b) for a six-step two-column PSA simulation. Steps are (1) co-current feed pressurization, (2) adsorption, (3) co-current pressure equalization depressurization, (4) counter-current blowdown, (5) counter-current purge, and (6) counter-current pressure equalization pressurization.

consumption was estimated assuming that the mixture CH_4/CO_2 was available at 1 bar and will be compressed to the feed pressure (4 bar), followed by further compression of the product (CH_4) to 200 bar. The specific use of energy in the PSA cycle is given by the blowdown and purge steps.

The existence of different cycle steps implies that different boundary conditions exist to solve the mathematical model presented previously. The different boundary conditions for each of the steps employed in the PSA cycle as well as initial conditions are listed in Table 3. In this study, it was assumed that the adsorption beds were at constant temperature (323 K) filled with an inert gas at a pressure of 1.2 bar.

The model described by eqs 6−14 using boundary and initial conditions provided in Table 3 was solved using gPROMS software (PSE Enterprise, U.K.). The centered finite difference method (CFDM) of second order over a uniform grid of 250 intervals was the numerical method used. The solvers employed in the simulations use a value of 1×10^{-5} for absolute tolerance.

3. PSA Simulation Results

3.1. PSA Sizing. The purpose of this work is to design a PSA unit for biogas upgrading and evaluate the effect of recycling streams in purge and equalization steps with some content of contaminant (CO_2). The biogas stream has a total flow rate of 500 N m^3/day (at 296.15 K and 1 atm) with a content of CO_2 of 33% balanced by CH_4. The biogas is available at 323 K and at atmospheric pressure and should be compressed to the feed pressure (4 bar).

The diameter of the PSA process was designed in order to have superficial velocity lower than 0.2 m/s in the feed step in order to allow a reasonable gas solid contact time and reduce effects of axial dispersion. The length of the column was fixed to have a feed time shorter than 10 min. All other properties of the column as well as the physical properties of the adsorbent are described in Table 4. The simulations were also carried out assuming that the columns will operate under adiabatic behavior ($U = 0$). However, some heat is exchanged with the column wall ($h_w = 35$ W/m^2 K). Under this regime, temperature excursion within the column (due to adsorption/desorption) will be the highest attainable and thus will establish a lower limit of operation: if there is some energy exchange with the surroundings, the temperature excursion will be smaller and PSA performance will be better.

As an example of the behavior of the column, in Figure 4, the simulation of a breakthrough curve for CH_4/CO_2 stream is presented. During the bulk CO_2 adsorption within the column, the temperature increase is higher than 60 K. The adiabatic behavior also produces a second plateau in the molar flow rate profile of CO_2.[62] The higher temperature within the bed resulted in a decreased overall capacity.

3.2. Simulation of One-Column PSA. The initial assessment of the behavior of a PSA process for CH_4/CO_2 separation was carried out by making simulations of the performance of one column. Simulations are quite fast (less than 3 h) to achieve cyclic steady state (more than 85 cycles), and thus, it is possible to fix step times to achieve high purity methane. These fast simulations also give us the basic knowledge of the system under study: which are the most important variables, which step or operating variable is the most sensitive one, and so forth.

An example of the results obtained in one-column simulation is depicted in Figure 5. The operating conditions of this example are listed in Table 5 (simulation 21). The pressure history of this cycle in cyclic steady state (CSS) is shown in Figure 2. According to the molar flow rate of gases exiting the column, it can be observed that desorption of CO_2 in the blowdown step corresponds to almost 50% while the rest of the CO_2 desorbs in the purge step. This indicates that the purge step is very important in achieving high purity methane. In previous simulations at lower temperature (306 K),[12,13] the nonlinearity of the CO_2 isotherms is so strong that very small amounts of CO_2 could be desorbed in the purge step. It can be also noted that some CO_2 is exiting the column in the depressurization step. If this stream is recycled, this behavior should be avoided by reducing the feed time. Also note that the time of the pressure

Table 3. Boundary and Initial Conditions of a PSA Process for CO_2/CH_4 Separation Employing Zeolite 13X

co-current pressurization with feed

inlet, $z = 0$	$z = Lc$
$-\frac{\varepsilon D_{ax}}{u(0)}\frac{\partial y(i,0)}{\partial z}_{z^+} + y(i,0)_{z^+} - y(i,0)_{z^-}$	$\frac{\partial y(i,Lc)}{\partial z}_{z^-} = 0$
$-\lambda\frac{\partial T_g(0)}{\partial z}_{z^+} + u\tilde{C}C_p T_g(0)_{z^+} - u\tilde{C}C_p T_g(0)_{z^-}$	$\frac{\partial T_g(Lc)}{\partial z}_{z^-} = 0$
$P(0) = P_{inlet}$	$u(Lc) = 0$

feed

inlet, $z = 0$	outlet, $z = Lc$
$-\frac{\varepsilon D_{ax}}{u(0)}\frac{\partial y(i,0)}{\partial z}_{z^+} + y(i,0)_{z^+} - y(i,0)_{z^-}$	$\frac{\partial y(i,Lc)}{\partial z}_{z^-} = 0$
$-\lambda\frac{\partial T_g(0)}{\partial z}_{z^+} + u\tilde{C}C_p T_g(0)_{z^+} - u\tilde{C}C_p T_g(0)_{z^-}$	$\frac{\partial T_g(Lc)}{\partial z}_{z^-} = 0$
$u(0)C(i,0)_{z^+} = u(0)C(i,0)_{z^-}$	$P(Lc) = P_{outlet}$

counter-current blowdown

outlet, $z = 0$	$z = Lc$
$\frac{\partial y(i,0)}{\partial z}_{z^+} = 0$	$\frac{\partial y(i,Lc)}{\partial z}_{z^-} = 0$
$\frac{\partial T_g(0)}{\partial z}_{z^+} = 0$	$\frac{\partial T_g(Lc)}{\partial z}_{z^-} = 0$
$P(0) = P_{low} + (P_E - P_{low})\exp(-k_{blow}t)$	$u(Lc) = 0$

counter-current purge

outlet, $z = 0$	inlet, $z = Lc$
$\frac{\partial y(i,0)}{\partial z}_{z^+} = 0$	$-\frac{\varepsilon D_{ax}}{u(0)}\frac{\partial y(i,Lc)}{\partial z}_{z^+} + y(i,Lc)_{z^+} - y(i,Lc)_{z^-}$
$\frac{\partial T_g(0)}{\partial z}_{z^+} = 0$	$-\lambda\frac{\partial T_g(Lc)}{\partial z}_{z^+} + u\tilde{C}C_p T_g(Lc)_{z^+} - u\tilde{C}C_p T_g(Lc)_{z^-}$
$P(0) = P_{outlet}$	$u(Lc)C(i,Lc)_{z^+} = u(Lc)C(i,Lc)_{z^-}$

pressure equalization (depressurization)

$z = 0$	outlet, $z = Lc$
$\frac{\partial y(i,0)}{\partial z}_{z^+} = 0$	$\frac{\partial y(i,Lc)}{\partial z}_{z^-} = 0$
$\frac{\partial T_g(0)}{\partial z}_{z^+} = 0$	$\frac{\partial T_g(Lc)}{\partial z}_{z^-} = 0$
$u(0) = 0$	one-column simulations, $P(0) = P_E + (P_{low} - P_E)\exp(-k_{blow\_eq}t)$
$u(0) = 0$	two-column simulations, $P(Lc) = P_{outlet}$

pressure equalization (pressurization)

$z = 0$	inlet, $z = Lc$
$\frac{\partial y(i,0)}{\partial z}_{z^+} = 0$	$-\frac{\varepsilon D_{ax}}{u(0)}\frac{\partial y(i,Lc)}{\partial z}_{z^+} + y(i,Lc)_{z^+} - y(i,Lc)\Big\vert_{z^-}$
$\frac{\partial T_g(0)}{\partial z}_{z^+} = 0$	$-\lambda\frac{\partial T_g(Lc)}{\partial z}_{z^+} + u\tilde{C}C_p T_g(Lc)_{z^+} - u\tilde{C}C_p T_g(Lc)_{z^-}$
$u(0) = 0$	$u(Lc)\,C(i,Lc)_{z^+} = u(Lc)\,C(i,Lc)_{z^-}$

initial conditions

$$q(i,z) = 0$$
$$T_g(z) = T_s(z) = T_w(z) = 323\ \text{K}$$
$$y(CO_2,z) = y(CH_4,z) = 0; \quad y(He,z) = 1$$
$$P(z) = 1.2\ \text{bar}$$

Table 4. Physical Properties of Adsorbent, Column Characteristics, and Operating Conditions Used in the Breakthrough and PSA Simulations

column length (m)	1.35
column radius (m)	0.10
column porosity	0.37
column wall specific heat (J kg^{-1} K^{-1})	500
column density (kg m^{-3})	834.12
column wall density (kg m^{-3})	8238
pellet density (kg m^{-3})	1324
pellet porosity	0.338
pellet radius (m)	0.0006
pellet tortuosity	2.0
mean pore radius (A)	243[a]
zeolite 13X specific heat (J $kg^{-1}K^{-1}$)	900
feed flow rate (SLPM)	347.2
pressure feed (bar)	4.0
temperature feed (K)	323.15

[a] Obtained by mercury intrusion porosimetry.

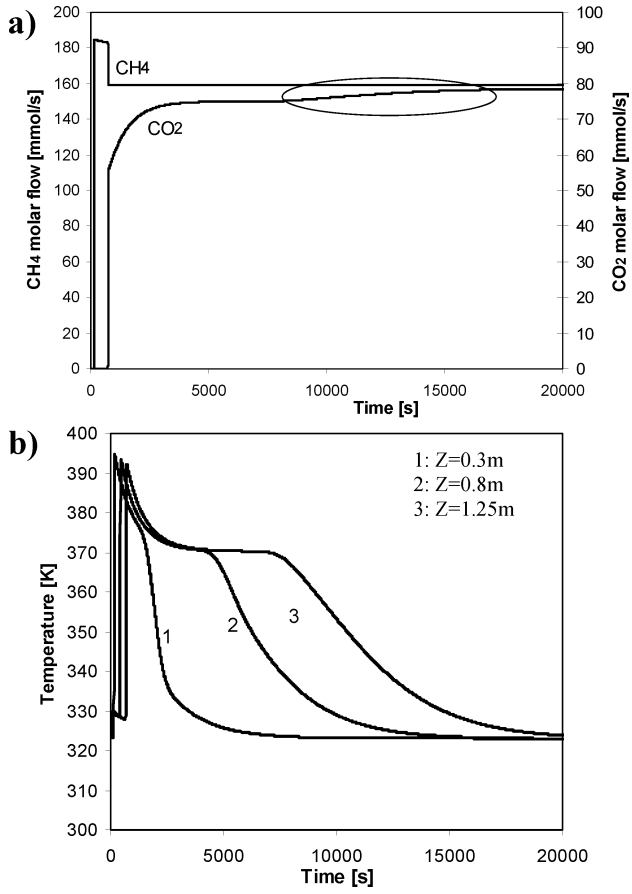

Figure 4. (a) Molar flow rate of CH_4 and CO_2 and (b) temperature profiles at 0.3, 0.8, and 1.25 m from feed inlet for a simulated binary curve (67% of CH_4 balanced by CO_2) at 323 K, 4 bar with a total feed flow rate of 347.2 SLPM. Other column properties are listed in Table 4.

equalization steps was fixed in 25 s to accommodate pressure changes without important variations in velocity reducing risks of particle damage by attrition.

The temperature increase (due to adsorption of CO_2) for different positions is also shown in Figure 5. When the temperature increases, the loading of CO_2 in the column also decreases considerably (see Figure 5c). Another important issue relating the good performance of this process at 323 K is the amount of CH_4 adsorbed in the column (Figure 5d). At lower temperatures, the amount of CH_4 adsorbed in the pressurization step is considerable (around 0.9 mol/kg), thus requiring larger amounts of CH_4, reducing unit productivity (and product recovery). When temperature is increased to 323 K, the amount of CH_4 adsorbed in the pressurization step is less than 0.4 mol/kg.

Different simulations were performed, and the results are summarized in Table 5. Two important conclusions can be taken from comparison with previous results.[12,13] Operating at higher temperature resulted in higher product recovery (and thus unit productivity) and also in significant power savings. The low power consumption is related to the pressure of the blowdown step employed: 0.3 bar instead of 0.1 bar used in previous works.[12,13]

Other important findings are related to the influence of specific variables such as feed pressure, purge flow rate, purge step time, blowdown pressure, and feed time. As shown in Figure 6, increasing the purge flow rate results in almost linear drop in product recovery (and unit productivity) without important impacts in CH_4 purity. On the other side, for a constant purge flow rate (see Figure 7), increasing the purge time has important impact on product purity (from 98% to 99%) with losses in recovery of 2%. Other important variables to take into account are the operating pressures (feed and blowdown). Increasing the blowdown pressure to values higher than 0.3 bar resulted in low-purity CH_4 by incomplete desorption of CO_2. Simulations carried out at higher feed pressure resulted in higher purity and lower recovery. The optimal feed pressure should be established from comparison of results at same product purity and overall power consumption.

In these one-column simulations, the CH_4 purity obtained is quite high. This is a consequence of the operation at higher temperatures: less nonlinear isotherms and faster diffusion make purge more effective. However, the second reason for this high purity is due to one specification in the simulations: the gas employed in the purge step and pressure equalization is pure methane.

3.3. Simulation of Two-Column PSA. It has been shown that, in the simulations of one-column PSA, product purity around 99% can be obtained. However, in real systems, recycling a stream with 1% of CO_2 to the product end will result in higher contamination of the product stream. An apparent solution is to use a partially contaminated stream in the simulations. However, the CO_2 content of these streams should be fixed from the first cycle and may not lead to the correct results. To obtain more realistic results, the performance of all the columns should be taken into account.

For a direct comparison of the results of simulating the process with one and two-columns, we will employ the same operating conditions as in simulation 21 (Table 5) and perform the simulation of a two-column PSA process. The result of the two-column process simulation is presented in Table 6. The pressure history of this cycle is shown in Figure 3. Please note that, when using this cycle, the initial guess for the pressure attained in the depressurization step is the intermediate value between feed and blowdown pressures. This assumption is valid if none of the recycled gases are adsorbed in the zeolite. However, since methane and the small amount of CO_2 recycled are adsorbed, the final pressure is lower than this intermediate value. In the molar flow rate of gases exiting the column, there are important differences in the results obtained with simulations of one-column (Figure 5a) and two-columns (Figure 8a). Note that, in the cyclic steady state (CSS) of the two-column simulation, when feed starts, there is some CO_2 exiting the column. This effect results from the recycling of contaminated streams both in purge and in pressure equalization steps. The presence of CO_2 at the end of the column can be observed in

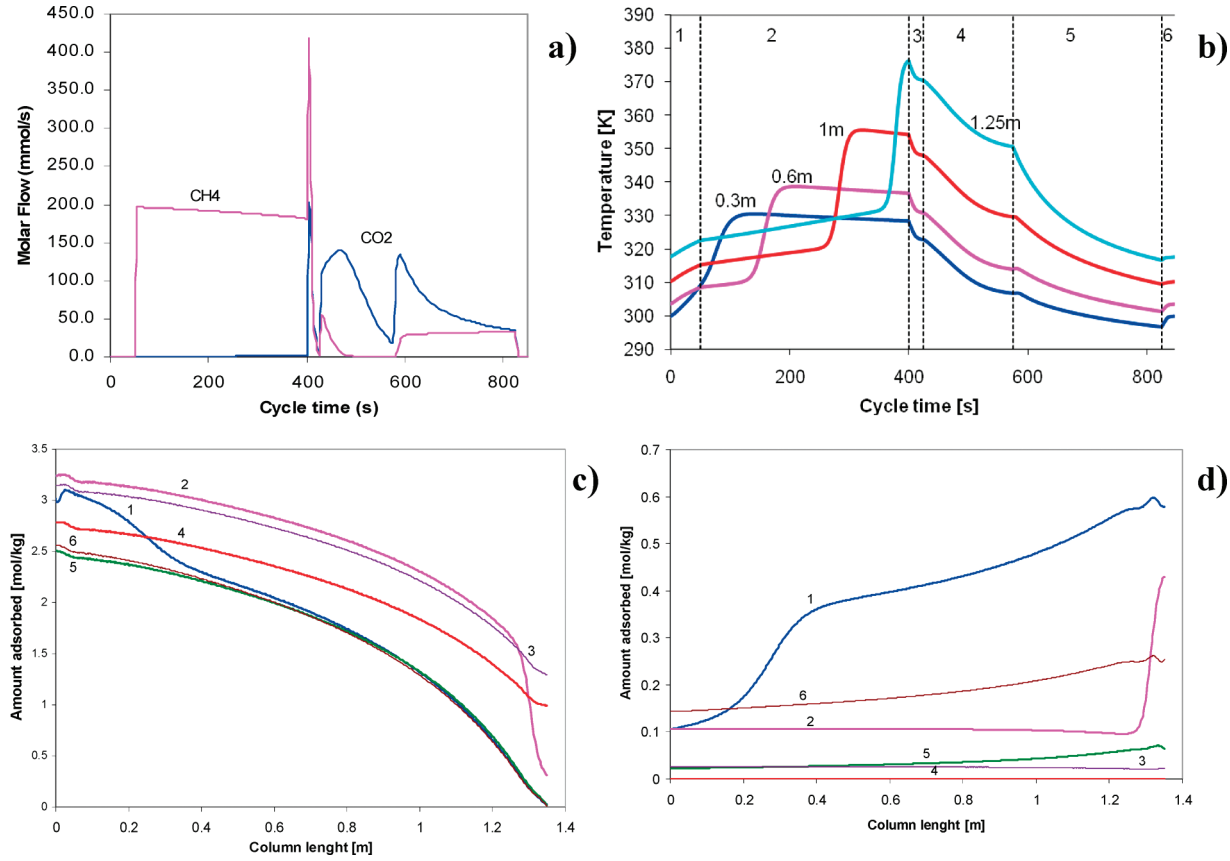

Figure 5. One-column simulation of PSA for CH_4-CO_2 separation using zeolite 13X. Cycle scheme is shown in Figure 2 and operating conditions in Table 5 (simulation 21). Results presented are (a) molar flow rate of each gas exiting the column, (b) temperature histories at different positions (0.3, 0.6, 1, and 1.25 m) from feed inlet, for cyclic steady state, amount adsorbed of (c) CO_2 and (d) CH_4. Numbers in the figures correspond to the different cycle steps: (1) co-current feed pressurization, (2) adsorption, (3) co-current pressure equalization depressurization, (4) counter-current blowdown, (5) counter-current purge, and (6) counter-current pressure equalization pressurization.

Table 5. One-Column PSA Performance for CH_4-CO_2 Separation Using Zeolite 13X with Modified Skarstrom Cycle[a]

simulation	t_{press} (s)	t_{feed} (s)	t_{blow} (s)	t_{purge} (s)	Q_{purge} (SLPM)	P_{high} (bar)	P_{low} (bar)	L/D	CH_4 purity	CH_4 recovery	CH_4 productivity (mol/kg h)	power (kW/mol)
3	50	350	200	200	104.16	4.0	0.3	6.75	99.73	70.34	5.38	0.149
4	50	350	200	200	86.8	4.0	0.3	6.75	99.63	74.17	5.67	0.140
5	50	350	200	200	69.44	4.0	0.3	6.75	99.46	78.05	5.97	0.13
6	50	350	200	200	52.08	4.0	0.3	6.75	98.75	81.79	6.26	0.12
7	50	350	200	200	52.08	8.0	0.3	6.75	99.56	76.69	5.87	0.138
8	50	350	200	200	52.08	3.0	0.3	6.75	95.96	82.59	6.32	0.122
9	50	350	200	200	52.08	4.0	0.5	6.75	91.25	82.33	6.30	0.113
10	50	350	200	200	52.08	4.0	0.7	6.75	86.21	82.79	6.33	0.110
11	50	350	200	200	52.08	4.0	0.3	2	99.09	81.77	6.25	0.124
12	50	350	200	200	52.08	4.0	0.3	16	96.29	81.84	6.26	0.124
13	50	375	200	200	52.08	4.0	0.3	6.75	96.49	82.92	6.55	0.116
14	50	330	200	200	52.08	4.0	0.3	6.75	99.28	80.17	5.97	0.133
15	50	350	180	200	52.08	4.0	0.3	6.75	98.80	81.79	6.40	0.125
16	50	350	220	200	52.08	4.0	0.3	6.75	98.82	81.78	6.11	0.123
17	50	350	200	180	52.08	4.0	0.3	6.75	97.97	82.81	6.49	0.123
18	50	350	200	220	52.08	4.0	0.3	6.75	99.27	80.64	5.88	0.120
19	40	350	200	200	52.08	4.0	0.3	6.75	98.85	81.76	6.49	0.121
20	60	350	200	200	52.08	4.0	0.3	6.75	98.78	81.80	6.18	0.124
21	50	350	150	250	52.08	4.0	0.3	6.75	99.55	78.67	6.02	0.130

[a] Depressurization and equalization time last 25 s.

Figure 8c where more CO_2 is adsorbed at the end of the depressurization step. Also, the amount of CO_2 in the purge does not start from zero since some gas is being recycled and adsorbed in the last layer of adsorbent. The opposite effect is observed in methane loading (Figure 8d): less methane is adsorbed since CO_2 is preferably adsorbed. Since we are recycling some CO_2 in the regeneration steps, the temperature increase in the column during the feed step is slightly smaller. In the two-column simulations, cyclic steady state is achieved only after 95 cycles: the recycling of CO_2 also added a delay in achieving CSS.

It can be observed that when contaminated streams are recycled, the product purity is smaller. However, since we are using a pressure equalization step, there is a significant increase in product recovery (and thus unit productivity). The power consumption per mole is smaller due to the higher productivity; same power consumption with more moles of methane produced.

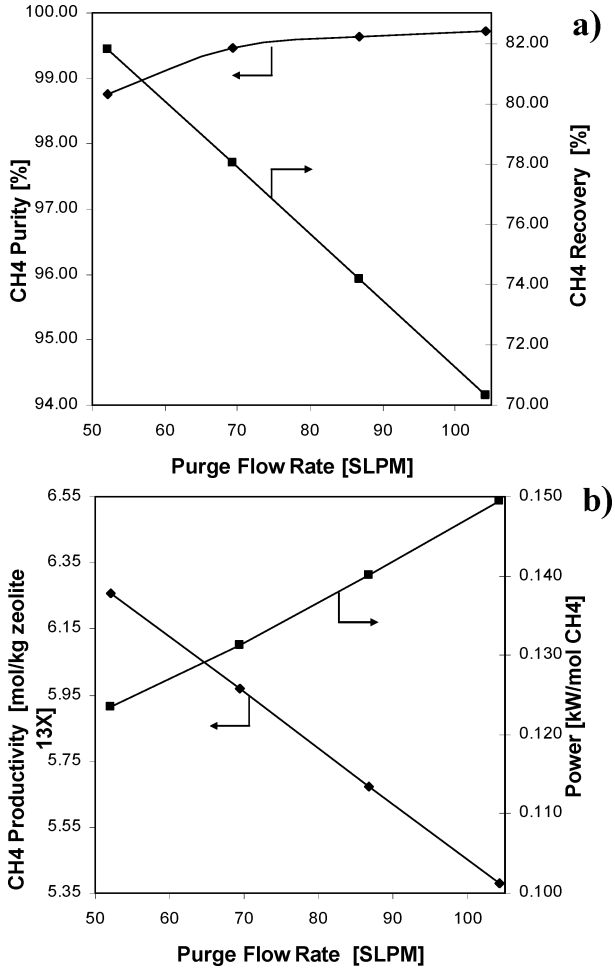

Figure 6. Effect of purge flow rate in one-column PSA performance: (a) CH_4 purity and recovery and (b) unit productivity and power consumption.

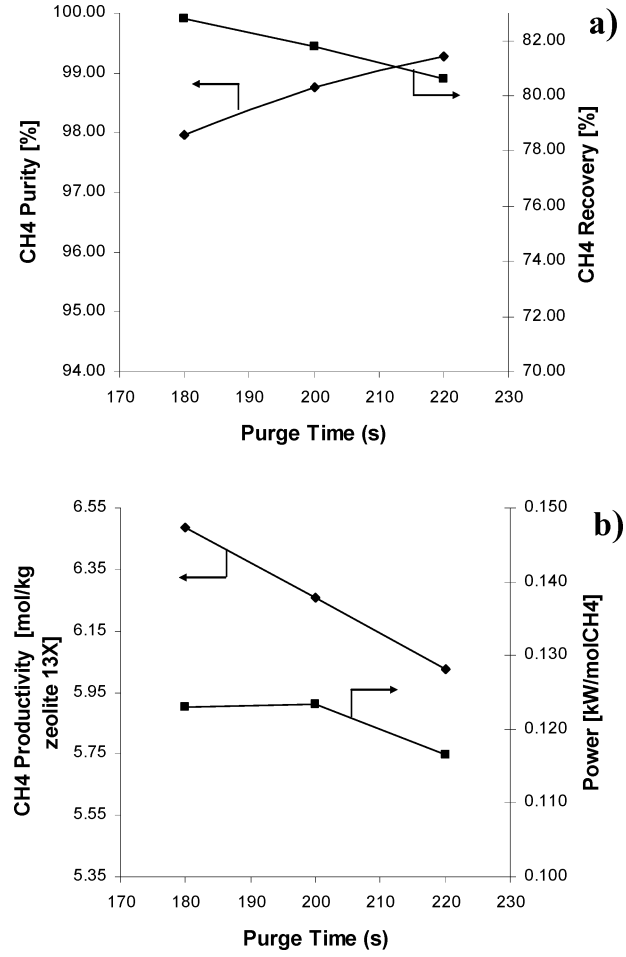

Figure 7. Effect of purge time in one-column PSA performance: (a) CH_4 purity and recovery and (b) unit productivity and power consumption.

Finally, the effect of recycling gas streams from one column to the other was evaluated in detail. For this purpose, we have defined all variables in the PSA cycle and vary the amount of feed that the process can admit in the pressurization and feed steps. The results can be observed in Figure 9. It is clear that when the methane purity is high (>99.5%), simulating a PSA process with one-column or with two-columns will result in very similar results of product purity and power consumption. However, when the methane purity decreases to values between 99.5 and 99.0%, larger differences arise from simulating one-column and the overall process. In this particular case, if we make simulations of one-column and obtain a product purity of 98%, when the process is scaled and more than one column is used, much smaller product purity will be obtained.

Simulations of the two-column process indicate that CH_4 purity > 99% can be obtained with product recovery around 85%. In order to increase the methane recovery, other columns should be employed with further pressure equalization steps.

4. Conclusions

The use of zeolite 13X in pressure swing adsorption for biogas upgrading was studied. We have determined adsorption equilibrium in a commercial sample of zeolite 13X and then conducted simulations of the PSA process for CH_4-CO_2 separation operating at 323 K which are exiting conditions of thermophilic digesters. A six-step PSA cycle comprising pressurization, feed, depressurization, blowdown, purge, and pressure equalization was employed. Operating at 323 K, the equilibrium isotherm is not very steep and purge can effectively remove CO_2. Unit productivity around 6 mol/kg

Table 6. Comparison between the Predicted Performance of the Studied PSA Employing One-Column and Two-Column Simulations[a]

	simulation	Q_{feed} (SLPM)	CH_4 purity	CH_4 recovery	CH_4 productivity (mol/kg h)	power (kW/mol)
a	1 bed	295.12	99.93	72.51	4.71	0.142
	2 bed	295.12	99.84	83.52	5.43	0.123
b	1 bed	313.52	99.74	75.07	5.19	0.137
	2 bed	313.52	99.22	85.04	5.87	0.121
c	1 bed	329.84	99.61	76.95	5.59	0.133
	2 bed	329.84	97.93	86.01	6.25	0.120
d	1 bed	347.2	99.55	78.67	6.02	0.130
	2 bed	347.2	96.02	86.86	6.64	0.117
e	1 bed	364.56	99.19	80.13	6.44	0.127
	2 bed	364.56	93.96	87.59	7.03	0.116
f	1 bed	373.24	98.51	80.60	6.63	0.126
	2 bed	373.24	92.96	87.94	7.23	0.115
g	1 bed	381.92	97.66	81.00	6.82	0.125
	2 bed	381.92	92.01	88.29	7.43	0.115

[a] All simulations were performed with a purge flow rate of 52.08 SLPM and feed and blowdown pressures of 4 and 0.3 bar, respectively. Pressurization time was 50 s, feed time was 350 s, pressure depressurization and equalization time was 25 s, blowdown time was 150 s, and purge time was 250 s.

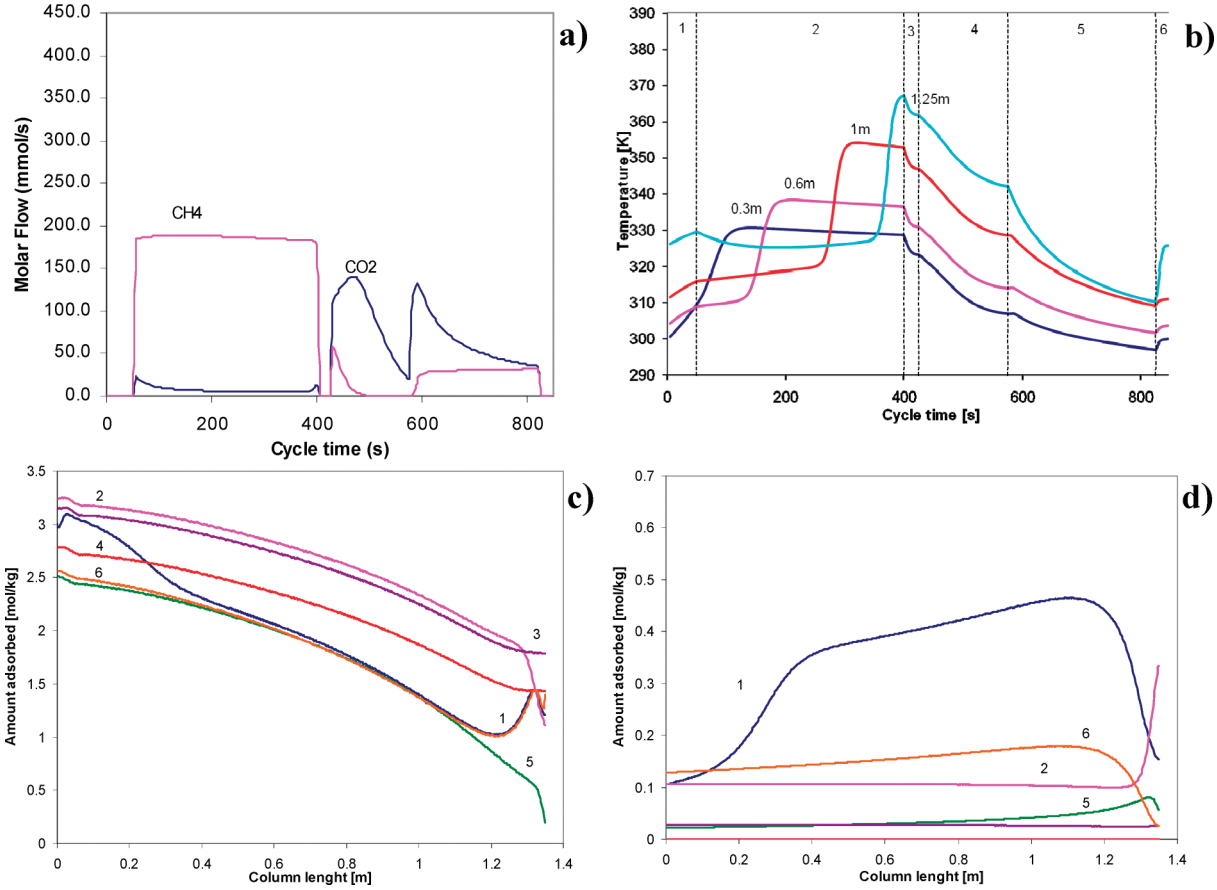

Figure 8. Two-column simulation of PSA for CH_4-CO_2 separation using zeolite 13X. Cycle scheme is shown in Figure 3 and operating conditions in Table 6 (simulation d, 2 bed). Results presented are (a) molar flow rate of each gas exiting the column, (b) temperature histories at different positions (0.3, 0.6, 1, and 1.25 m) from feed inlet, for cyclic steady state, amount adsorbed of (c) CO_2 and (d) CH_4. Numbers in the figures correspond to the different cycle steps: (1) co-current feed pressurization, (2) adsorption, (3) co-current pressure equalization depressurization, (4) counter-current blowdown, (5) counter-current purge, and (6) counter-current pressure equalization pressurization.

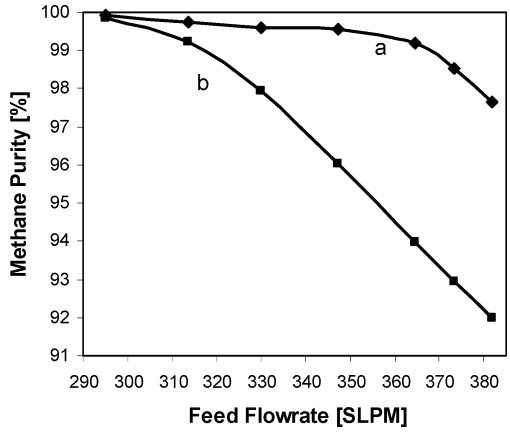

Figure 9. Simulation results for PSA cycle employing one and two columns with cycle scheme showed in Figures 2 and 3, respectively. The simulation conditions are detailed in Table 6. Effects in methane purity of feed flow rate for (a) one column and (b) two columns.

h was obtained with a power consumption of 0.12 kW/mol CH_4 produced.

The simulation of a two-column PSA process was also assessed. It was observed that when streams with more than 0.5% CO_2 are recycled in the purge and pressure equalization steps, there is a severe decrease in the methane purity obtained as product. The important benefit of using pressure equalization relies on the increase of product recovery which is always higher than 80%. With these two-column process simulations it was possible to find conditions to operate the PSA and produce methane with purity of 99.2%, recovery of 85.0% with a unit productivity of 5.9 mol CH_4/kg h, and a power consumption of 0.12 kW/mol CH_4 produced. Simulations including the recycle of dirty streams provide more realistic results than the ones obtained with simulations of one-column that should be only considered as accurate if high purity gases are recycled in purge and equalization steps.

Acknowledgment

The authors gratefully acknowledge the collaboration project with Methaneva SARL (France) to design small-sized PSA units for biogas upgrading. Both experimental observations and fruitful discussions with Dr. Patrice Renard (Methaneva President) allowed the improved operation of PSA units. M.P.S.S. acknowledges the research fellowship from project PDTC/EQU-EQU/65541/2006.

Notation

a_i = number of neighboring sites occupied by component i
a_p = particle specific area (m^{-1})
$\dot{B}$ = molar flowrate to be compressed
Bi_i = mass Biot number of component i
C_i = gas phase concentration of component i (mol m^{-3})
$\tilde{C}_p$ = molar constant pressure specific heat of the gas mixture (J mol-1 K-1)
$\tilde{C}_{ps}$ = constant volumetric specific heat of component i (J kg^{-1} K^{-1})

$\langle C_{p,i} \rangle$ = macropore averaged concentration of component i (mol m^{-3})
$\tilde{C}_{pw}$ = constant pressure specific heat of the column wall (J kg^{-1} K^{-1})
$\tilde{C}_{vi}$ = molar constant volumetric specific heat of component i (J mol^{-1} K^{-1})
$\tilde{C}_{v,ads,i}$ = molar constant volumetric specific heat of component i adsorbed (J mol^{-1} K^{-1})
d_p = particle diameter (m)
d_{wi} = wall internal diameter (m)
D = column diameter (m)
D_{ax} = axial dispersion coefficient (m^2 s^{-1})
$D_{k,i}$ = Knudsen diffusivity of component i (m^2 s^{-1})
$D_{m,i}$ = molecular diffusivity of component i (m^2 s^{-1})
$D_{p,i}$ = macropore diffusivity of component i (m^2 s^{-1})
e = wall thickness (m)
E_{ai} = activation energy of micropore diffusion of component i (J mol^{-1})
F_{CH_4} = number of CH_4 moles fed to the column in pressurization and feed steps (mol)
h_f = film heat transfer coefficient between the gas and the solid phase (W m^{-2} K^{-1})
h_w = wall heat transfer coefficient between the gas and the column wall (W m^{-2} K^{-1})
k_{blow} = constant for describing the time-evolution of variables and fluxes at boundaries, in the blowdown step (s^{-1})
k_{blow_eq} = constant for describing the time-evolution of variables and fluxes at boundaries, in the pressure equalization depressurization step (s^{-1})
k_f = film mass transfer coefficient (m s^{-1})
k_g = gas thermal conductivity (W m^{-1} K^{-1})
K_i = equilibrium constant of component i in the multisite Langmuir isotherm (Pa^{-1})
K_i^0 = equilibrium constant at the limit $T \rightarrow \infty$ of component i (Pa^{-1})
$K_{u,i}$ = micropore diffusivity of component i (m^2 s^{-1})
$K_{u,i}^0$ = limiting diffusivity at infinite temperature of component i (m^2 s^{-1})
L = column length (m)
M_w = molecular weight (kg mol^{-1})
N_{CH_4} = number of moles of CH_4 exiting the column in feed step (mol)
N_{CO_2} = number of moles of CO_2 exiting the column in feed step (mol)
Nu = Nusselt number
P = pressure (bar)
P_{low} = blowdown pressure (bar)
P_E = equalization pressure (bar)
P_{high} = discharge pressure (bar)
Pr = Prandtl number
$q_{max,i}$ = maximum adsorbed phase concentration of component i (mol kg^{-1})
$\langle \bar{q}_i \rangle$ = macropore averaged adsorbed phase concentration of component i (mol kg^{-1})
q_i^* = adsorbed phase in equilibrium with the average concentration in the macropores (mol kg^{-1})
Q_{feed} = feed flow rate (SLPM)
Q_{purge} = purge flow rate (SLPM)
r_p = pore radius (m)
R_{CH_4} = number of CH_4 moles used in pressurization and purge steps (mol)
Re = Reynolds number
R_g = universal gas constant (J mol^{-1} K^{-1})
R_p = particle radius (m)
R_w = radius of the column wall (m)
Sc = Schmidt number
Sh = Sherwood number
t = time (s)
t_{blow} = blowdown step time (s)
t_{feed} = feed step time (s)
t_{press} = pressurization step time (s)
t_{purge} = purge step time (s)
T_{feed} = feed temperature (K)
T_g = gas temperature (K)
T_s = solid phase temperature (K)
T_w = column wall temperature (K)
T_∞ = ambient temperature (K)
u_0 = superficial velocity (m s^{-1})
U = global external heat transfer coefficient (W m^{-2} K^{-1})
y_i = molar fraction of component i
z = axial position (m)

Greek Letters

α_w = ratio of the internal surface area to the volume of the column wall (m^{-1})
α_{wl} = ratio of the logarithmic mean surface area of the column shell to the volume of the column wall (m^{-1})
ε_c = bed porosity
ε_p = particle porosity
γ = equal to 3/2 for ideal gases
λ = heat axial dispersion coefficient (W m^{-2} K^{-1})
$\Delta H_{ads,i}$ = heat of adsorption of component i (J mol^{-1})
η = mechanical efficiency (assumes a value of 0.8)
μ = gas viscosity (Pa s) ρ_b bulk density (kg m^{-3})
ρ_g = gas density (kg m^{-3})
ρ_p = particle density (kg m^{-3})
ρ_w = column wall density (kg m^{-3})
τ_p = pore tortuosity

Literature Cited

(1) Pritchard, C. L. *Chasing the Dragon's Tail: Life Cycle Carbon Analysis Applied to CO_2 Sequestration*, 7th International Conference on Greenhouse Gas Control Technologies. Vancouver, Canada, September 5−9, 2004.

(2) Knaebel, K. S.; Reynhold, H. E. Landfill Gas: From Rubbish to Resource. *Adsorption* **2002**, *9*, 87–94.

(3) GHG Data; United Nations Framework Convention on Climate Change; http://unfccc.int/ghg_data/ghg_data_unfccc/items/4146.php (accessed March 2010).

(4) Foundation for Biotechnology Awareness and Education (FBAE); http://fbae.org/2009/FBAE/website/our-position-biofuel_potential-future-crop-of-farmers.html (accessed March 2010).

(5) Li, S.; Martinek, J. G.; Falconer, J. L.; Noble, R. D.; Gardner, T. Q. High pressure CO_2/CH_4 separation using SAPO-34 membranes. *Ind.Chem. Eng. Res.* **2005**, *44*, 3220–3228.

(6) Shin, H.-C.; Park, J.-W.; Song, H.-C. Removal characteristics of trace compounds of landfill gas by activated carbon adsorption. *Environ. Pollut.* **2002**, *119*, 227–236.

(7) Jacobsson, E. *Upgrading biogas to natural gas quality*, European Biomethane Fuel Conference, Göteborg, Sweden, September 7−9, 2009.

(8) Wellinger, A. *Gas upgrading issues*, European Biomethane Fuel Conference. Göteborg, Sweden, September 7−9, 2009.

(9) Air Liquide. Medal membrane technology brochure; http://www.medal.airliquide.com/en/co-membrane/co-membrane-technology.html (accessed March 2010).

(10) CarboTech. Carbon molecular sieves flyer; http://www.carbotech.de/pdf_viewer/pdf_view.php?pdf_file=carbotech_cms_folder_en.pdf (accessed March 2010).

(11) Xebec. Biogas purification PSA systems; http://www.xebecinc.com/products-biogas-purification.php (accessed March 2010).

(12) Grande, C. A.; Rodrigues, A. E. Biogas to Fuel by Vacuum Pressure Swing Adsorption I. Behavior of Equilibrium and Kinetic Adsorbents. *Ind. Eng. Chem. Res.* **2007**, *46*, 4595–4605.

(13) Grande, C. A.; Rodrigues, A. E. Layered Vacuum Pressure- Swing Adsorption for Biogas Upgrading. *Ind. Eng. Chem. Res.* **2007**, *46*, 7844–7848.

(14) Ruthven, D. M.; Farooq, S.; Knaebel, K. S. *Pressure Swing Adsorption*; Wiley-VCH: New York, 1994.

(15) Yang, R. T. *Gas Separation by Adsorption Processes*; Butterworths: Boston, 1987.

(16) Sircar, S.; Kock, W. R. Adsorptive Separation of Methane and Carbon Dioxide Gas Mixtures. European Patent EP 0193716, 1986.

(17) Sircar, S.; Kock, W. R. Adsorptive Separation of Gas Mixtures. European Patent EP 0257493, 1988.

(18) Davis, M. M.; Gray, R. L. J.; Patei, K. Process for the Purification of Natural Gas. U.S. Patent, US 5174796, 1992.

(19) Sircar, S.; Kumar, R.; Koch, W. R.; Vansloun, J. Recovery of Methane from Landfill Gas. U.S. Patent 4,770,676, 1988.

(20) Dolan, W. B.; Mitariten, M. J. CO_2 Rejection from Natural Gas. U.S. Patent US 2003/0047071, 2003.

(21) Müller, U. ; Hesse, M. ; Putter, H. ; Schubert, M.; Mirsch, D. Adsorptive Anreicherung von Methan in Methan-haltigen Gasmischen. European Patent EP 1674555, 2005.

(22) Cavenati, S.; Grande, C. A.; Rodrigues, A. E. Metal Organic Framework Adsorbent for Biogas Upgrading. *Ind. Eng. Chem. Res.* **2008**, *47*, 6333–6335.

(23) Masahiro, L.; Kazuo, H. Method for Removing Carbon Dioxide from Mixed Gas and Alternative Natural Gas Generating Device Using the Method. World Patent WO95526804, 1995.

(24) Seery, M. W. Bulk Separation of Carbon Dioxide from Methane Using Natural Clinoptilolite. World Patent WO 98/58726, 1998.

(25) Jayaraman, A.; Hernandez-Maldonado, A. J.; Yang, R. T.; Chinn, D.; Munson, C. L.; Mohr, D. H. Clinoptilolites for nitrogen/methane separation. *Chem. Eng. Sci.* **2004**, *59*, 2407–2417.

(26) Jayaraman, A.; Yang, R. T.; Chinn, D.; Munson, C. L. Tailored Clinoptilolites for Nitrogen/Methane Separation. *Ind. Eng. Chem. Res.* **2005**, *44*, 5184–5192.

(27) Dolan, W. B.; Mitariten, M. J. Heavy Hydrocarbon Recovery from Pressure Swing Adsorption Unit Tail Gas. U.S. Patent US 6,610,124, 2003.

(28) Anson, A.; Lin, C. C. H.; Kuznicki, S. M.; Sawada, J. A. Adsorption of carbon dioxide, ethane, and methane on titanosilicate type molecular sieves. *Chem. Eng. Sci.* **2009**, *64*, 3683–3687.

(29) Fujita, S.; Himeno, S.; Suzuki, K. Method for Concentrating Methane from Sewage Sludge and Methane Storage Equipment. European Patent EP 1,647,531,Al.

(30) Li, S.; Falconer, J. L.; Noble, R. D. Improved SAPO-34 Membranes for CO_2/CH_4 Separations. *Adv. Mater.* **2006**, *18*, 2601–2603.

(31) Cavenati, S.; Grande, C. A.; Rodrigues, A. E. Upgrade of Methane from Landfill Gas by Pressure Swing Adsorption. *Energy Fuels* **2005**, *19*, 2545–2555.

(32) Pilarczyk, E., Knoblauch, K., Li, N., Strathmann, H., Eds. *Separation Technology*; Engineering Foundation: New York, 1988; p 522.

(33) Schroter, H. J., Juntgen, H., Rodrigues, A. E., LeVan, M. D., Tondeur, D. , Eds. *Adsorption: Science and Technology*; NATO ASI; Kluwer: Dordrecht, 1989; Vol. 158, p 269.

(34) Kapoor, A.; Yang, R. T. Kinetic Separation of Methane - Carbon Dioxide Mixture By Adsorption on Molecular Sieve Carbon. *Chem. Eng. Sci.* **1989**, *44*, 1723–1733.

(35) Gomes, V. G.; Hassan, M. M. Coal-seam methane recovery by vacuum swing adsorption. *Sep. Purif. Technol.* **2001**, *24*, 189–196.

(36) Kim, M.-B.; Bae, Y.-S.; Choi, D. K.; Lee, C.-H. Kinetic Separation of Landfill Gas by a Two Bed Pressure Swing Adsorption Process Packed with Carbon Molecular Sieve: Nonisothermal Operation. *Ind. Eng. Chem. Res.* **2006**, *45*, 5050.

(37) Delgado, J. A.; Uguina, M. A.; Sotelo, J. L.; Ruíz, B.; Gómez, J. M. Fixed-bed adsorption of carbon dioxide/methane mixtures on silicalite pellets. *Adsorption* **2006**, *12*, 5–18.

(38) Delgado, J. A.; Uguina, M. A.; Sotelo, J. L.; Ruíz, B.; Rosário, M. Carbon Dioxide/Methane Separation by Adsorption on Sepiolite. *J. Nat. Gas Chem.* **2007**, *16*, 235–243.

(39) Bonnot, K.; Tondeur, D. Effects of Composition, Temperature and Purge on the Performance of the Cyclic Adsorption of CO_2 and CH_4 on Activated Carbon. *Chem. Eng. Res. Des.* **2006**, *84* (A3), 192–208.

(40) Delgado, J. A.; Uguina, M. A.; Sotelo, J. L.; Ruíz, B.; Rosário, M. Separation of carbon dioxide/methane mixtures by adsorption on a basic resin. *Adsorption* **2006**, *13*, 373–383.

(41) Skarstrom, C. W. Method and apparatus for fractionating gaseous mixtures by adsorption. U.S. Patent 2,944,627, 1960.

(42) Zupančič, G. D.; Roš, M. Heat and energy requirements in thermophilic anaerobic sludge digestion. *Renewable Energy* **2003**, *28*, 2255–2267.

(43) Marsh, W. D.; Pramuk, F. S.; Hoke, R. C.; Skarstrom, C. W. Pressure equalization depressurising in heatless adsorption. U.S. Patent 3,142,547, 1964.

(44) Berlin, N. H. Method for providing an oxygen-enriched environment. U.S. Patent 3,280,536, 1966.

(45) Wagner, J. L. Selective adsorption process. U.S. Patent 3,430,418, 1969.

(46) Warmuzinski, K. Effect of pressure equalization on power requirements in PSA systems. *Chem. Eng. Sci.* **2002**, *57*, 1475–1478.

(47) Delgado, J. A.; Rodrigues, A. E. Analysis of the Boundary Conditions for the Simulation of the Pressure Equalization Step in PSA Cycles. *Chem. Eng. Sci.* **2008**, *63*, 4452–4463.

(48) Siettos, C. I.; Pantelides, C. C.; Kevrekidis, I. G. Enabling Dynamic Process Simulators to Perform Alternative Tasks: A Time-Stepper-Based Toolkit for Computer-Aided Analysis. *Ind. Eng. Chem. Res.* **2003**, *42*, 6795–6801.

(49) Cavenati, S.; Grande, C. A.; Rodrigues, A. E. Separation of $CH_4/CO_2/N_2$ mixtures by layered Pressure Swing Adsorption for upgrade of natural gas. *Chem. Eng. Sci.* **2006**, *61*, 3893–3906.

(50) Lü, Y.; Doong, S.-J.; Bülow, M. Pressure-Swing Adsorption Using Layered Adsorbent Beds with Different Adsorption Properties: I—Results of process simulation. *Adsorption* **2003**, *9*, 337–347.

(51) Lü, Y.; Doong, S.-J.; Bülow, M. Pressure-Swing Adsorption Using Layered Adsorbent Beds with Different Adsorption Properties: II—Experimental Investigation. *Adsorption* **2004**, *10*, 267–275.

(52) Ribeiro, A. M.; Grande, C. A.; Lopes, F. V. S.; Loureiro, J. M.; Rodrigues, A. E. A parametric study of layered bed PSA for hydrogen purification. *Chem. Eng. Sci.* **2008**, *63*, 5258–5273.

(53) Nitta, T.; Shigetomi, T.; Kuro-Oka, M.; Katayama, T. An adsorption isotherm of multi-site occupancy model for homogeneous surface. *J. Chem. Eng. Jpn.* **1984**, *17*, 39–45.

(54) Sircar, S. Influence of Adsorbate Size and Adsorbent Heterogeneity on IAST. *AIChE J.* **1995**, *41*, 1135–1145.

(55) Ruthven, D. M. *Principal of Adsorption and Adsorption Processes*; John Wiley & Sons: New York, 1984.

(56) Da Silva, F. A. Cyclic Adsorption Processes: Application to Propane/Propylene Separation. Ph.D. Dissertation, University of Porto, Portugal, 1999.

(57) Wakao, N.; Funazkri, T. Effect of fluid dispersion coefficients on particle-to-fluid mass transfer coeficients in packed beds. *Chem. Eng. Sci.* **1978**, *33*, 1375–1384.

(58) Bird, R. B.; Stewart, W. E.; Lightfoot, E. N. *Transport Phenomena*, 2nd ed.; Wiley International: Singapore, 2002.

(59) Wasch, A. P. D.; Froment, G. F. Heat transfer in packed beds. *Chem. Eng. Sci.* **1972**, *27*, 567–576.

(60) Nikolic, D.; Giovanoglou, A.; Georgiadis, M. C.; Kikkinides, E. S. Generic Modeling Framework for Gas Separations Using Multibed Pressure Swing Adsorption Processes. *Ind. Eng. Chem. Res.* **2008**, *47*, 3156–3169.

(61) Nikolic, D.; Kikkinides, E. S.; Georgiadis, M. C. Optimization of Multibed Pressure Swing Adsorption Processes. *Ind. Eng. Chem. Res.* **2009**, *48*, 5388–5398.

(62) Basmadjian, D. *The Little Adsorption Book: A Practical Guide for Engineers and Scientists*; CRC Press: Boca Raton, FL, 1997.

Received for review March 30, 2010
Revised manuscript received July 22, 2010
Accepted November 30, 2010

IE100757U